WORLD CONFERENCE ON TIMBER ENGINEERING 2025
BRISBANE, AUSTRALIA
Advancing Timber for the Future Built Environment

DEVELOPMENT OF UHPC NODES FOR TIMBER STRUCTURES

A. Abdallah [1], M. Shahnewaz [2], C. Dickof [3], L. Tobber [4]

ABSTRACT: The mass timber structures are becoming more commonplace as sustainable systems. During fire incidents, however, the conventional metallic connectors often become the weakest link, compromising structural integrity. To overcome this, innovative precast ultra-high-performance concrete (UHPC) nodes has been introduced. This paper introduces the concept, UHPC fabrication procedures, and experimental evaluation of UHPC nodes tested at Fast + Epp's Concept Lab in Vancouver, Canada. Finite-element models (FEM) in ABAQUS were validated against tests. A parametric study was performed, followed by additional tests to evaluate the efficiency and performance of deformed rebars in the proposed nodes. The test results showed a high potential of UHPC nodes, with an increase in capacity up to 243% with the addition of rebars. The parametric study showed that node geometry, presence of steel bar as well as FEM material model parameters significantly influence the performance of the UHPC nodes. Furthermore, this study also proposes analytical models to estimate the load-bearing capacity of the UHPC nodes.

KEYWORDS: timber, ultra-high-performance concrete (UHPC), corbel, beam-column joint, finite-element

1 – INTRODUCTION

Mass timber has been extensively used over the last two decades to help meeting the increasing growth of urbanization while maintaining sustainable construction techniques. Reducing the carbon footprint of the building, having a high strength-to-weight ratio and. Enhanced speed and efficiency of construction are amongst their advantages.

A modern example of mass timber structures equipped with energy dissipators, marking the tallest timber braced frame structure in North America upon its completion, is *The Hive* (formerly known as *Keith Drive*) office building in Vancouver [1], as shown in Fig. 1. Metallic connectors were utilized at the beam-column joints and columns-to-column joints.

While the mass timber members can exhibit adequate fire rating thanks to charring of their outer layers, the metallic connectors are vulnerable at elevated temperatures [2]. This, in turn, may necessitate concealing of such connections, which adds up to the cost and complexity of building erection.

This paper introduces a novel precast UHPC node for mass timber buildings. An overview of the node and details of experimental program conducted at Fast + Epp's Concept Lab is presented, followed by numerical study using finite-element models (FEM) in ABAQUS [3]. Analytical models were developed using the results of the experiments and FEMs. Key findings from the experimental, numerical and analytical work are summarized, followed by conclusions and recommendations for future work.

Figure 1: Rendering of The Hive (formerly Keith Drive) office building in Vancouver (courtesy of DIALOG and Fast + Epp)

2 – THE NODE CONCEPT

[1] Amr Abdallah, University of British Columbia, Kelowna, Canada, abdalla3@myumanitoba.ca

[2] Md Shahnewaz, Fast + Epp, Vancouver, Canada, mshahnewaz@fastepp.com

[3] Carla Dickof, Fast + Epp, Vancouver, Canada, cdickof@fastepp.com

[4] Lisa Tobber, University of British Columbia, Kelowna, Canada, lisa.tobber@ubc.ca

https://doi.org/10.52202/080513-0421

While several studies were conducted on timber-concrete composite systems [4-5], limited research reported on the use of concrete nodes at timber joints. Plain concrete nodes along with steel anchors were studied by Hartig et al. [6] for timber trusses. Similarly, Negrão et al. [7] tested cast-in-place reinforced concrete knee joints for timber post-and-beam structures. For the aforementioned studies, the use of concrete provided efficient concealing of the metallic connectors from fire hazard, promoting a substantially improved structural performance.

The initial concept of the node is visualized to be in mass timber gravity load-resisting frame as shown in Fig. 2, at a beam-column joint on an intermediate story, where glulam beams are supported in one direction only without having transverse beams, since the mass timber floor system spans one-way only. Bottom notches to be created in the glulam beams to create an aesthetically appealing view for the final structure with a smooth beam soffit without any drops. Post-installed steel anchors are used to carry any potential accidental lateral load as per Clause 27.1.4 of CSA S16-19 [8], maintaining the structural integrity of the structure. Fig. 2a depicts an isolated beam-column joint containing the precast node.

Ultra-high performance concrete (UHPC) was selected for the nodes to overcome some limitations associated with normal- or high-strength concrete are used in the proposed nodes, reinforcing bars, ties and framing bars are required, resulting in bar congestion and additional labour and time. Also, large corbel (i.e., the projecting concrete part that carries the timber beams, while the *node* refers to the whole unit: the two corbels and the part in between) depths and notched glulam beam with screw shear reinforcement are expected. Furthermore, limited edge distance and spacing for the post-installed anchors may be required. Therefore, UHPC was selected for the nodes to overcome such limitations owing to its superior mechanical properties, ductility and durability. Its enhanced compressive strength allows smaller cross-sections to be used. This can result in shallower corbels without screw shear reinforcing of the notched glulam beams, promoting aesthetics, particularly when the node is concealed within the timber joint. Also, the improved tensile properties of UHPC due to presence of fibres can eliminate the need for stirrups in addition to reduced longitudinal bars [9]. This approach has been successfully implemented in the first field application of UHPC nodes in the Marpole-Oakridge Community Centre in Vancouver, Canada as shown in Fig. 2b. Being a strong base material, UHPC facilitates post-installed steel anchors with significantly smaller embedment depths, edge distance and spacing requirements [10], contributing to more compact nodes. Moreover, the small-sized UHPC nodes within the structure indicates a small quantity of UHPC at a lower cost compared to traditionally used proprietary metallic connectors, as per a preliminary cost analysis.

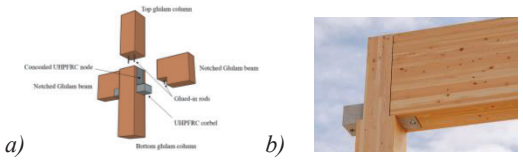

a) *b)*

Figure 2: Conceptual view of UHPC node in a post-and beam timber structure (photo courtesy of Fast + Epp's Concept Lab)

2.1 EXISTING ANALYTICAL MODELS

As the tested nodes exhibited flexural failure, as discussed later in more detail, the load-carrying capacities of the FEMs without steel bars are estimated by treating the nodes as prisms subjected to four-point bending, utilising the experimentally established flexural strength of the UHPC mix as follows.

$$P_{flex} = \frac{fbh^2}{3a} \quad (1)$$

where P_{flex} is the predicted load, f is the flexural strength, b and h refer to the average width and depth of the specimen, respectively, and a is the shear span.

Additionally, the flexural model proposed by Fattuhi [11] **is** employed to estimate the load capacities of the FEMs, as recommended by Ridha et al. [12]. This model is based upon force equilibrium between concrete in the compression zone and concrete in the tension zone plus reinforcing bars, if any. The tensile stresses in concrete are simplified as uniform tensile stress using the factor k_o factor, which is set as 0.353 by Fattuhi [11].

For the nodes reinforced with steel bars, the load capacity was predicted using the method outlined by El-Helou and Graybeal [13] for UHPC flexural members. This model assumes force equilibrium between UHPC in compression against UHPC in tension along with steel bars. Since all tested finite element models (FEMs) failed due to steel bar rupture, as demonstrated later in more detail, it was assumed that the cross-section fails by steel bar rupture while the UHPC at the extreme tension fibre reaches the localisation strain, $\varepsilon_{t,loc}$., and UHPC under compression reaches a value lower than f'_c estimated through strain compatibility. Furthermore, the reduction factor for the tensile strengths of the UHPC, γ, was set to unity to reflect controlled laboratory conditions.

3 – EXPERIMENTAL WORK

3.1 UHPC PROPERTIES AND SPECIMEN DETAILS

The experimental program was conducted in two phases; where eighteen nodes were cast and tested in the first

https://doi.org/10.52202/080513-0421

phase [14], followed by a numerical and parametric study before the second phase of experimental testing of six additional nodes. The test specimens resembled the beam-column joints of a mass timber gravity load-resisting frame. For the first phase of testing, the nodes were tested without steel bars or ties. In phase 2, three nodes were reinforced with steel ties in the longitudinal direction and three nodes were tested without steel reinforcement. The test specimens are described in Table 1 and Fig. 3 illustrates the geometry and cross section of the specimens. The testing program commenced with specimens S-100-100-150 and X-100-100-150 to evaluate the impact of the lower column stub (i.e., upper column stub due to the inverted loading scheme), which usually exists in other experimental studies [12]. No lower stubs were included for the rest of the test matrix. The investigated parameters were the thickness, shear span, and width of the corbels for the first series of specimens, whereas the only variable tested in the second phase was the presence of longitudinal steel bars in the corbels. For each variable, three identical nodes were cast to allow for any potential scatter of the results. As can be observed in Table 1, each three identical replicates were given a letter denoting their group (A to H).

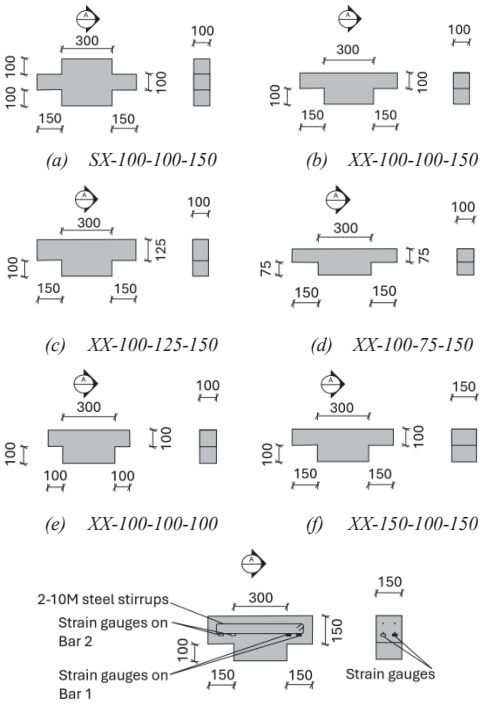

(a) SX-100-100-150 *(b) XX-100-100-150*

(c) XX-100-125-150 *(d) XX-100-75-150*

(e) XX-100-100-100 *(f) XX-150-100-150*

(g) XR-150-150-150

Figure 3: Details of tested UHPC nodes [14] – all dimensions are in mm.

A proprietary UHPC mix ce200SF-G^{TM} [15], with a target 28-day compressive strength of 130 MPa, was used to cast the nodes. The components and mixing proportions of the UHPC mix used for each phase are listed in Table 2. Prior to casting the node specimens and material samples, a flow test was conducted as per ASTM C1856 [16], where the average flow diameter was approximately 240 and 225 mm, for the first and second phases, respectively. In addition to casting the nodes, two sets of 75 × 150-mm cylinders and prisms [17] were cast to assess the compressive and flexural strength of the hardened UHPC, respectively. The mechanical properties of hardened UHPC are summarized in Table 3.

Table 1: Details of the UHPC node specimens

Phase	Specimen ID		Lower Column Stub	Steel Bars	Corbel Dimension (mm)		
					Width	*Thickness*	*Length*
1	A1	SX-100-100-150	Yes		100	100	150
	A2						
	A3						
	B1	XX-100-100-150			100	100	150
	B2						
	B3						
	C1	XX-100-125-150			100	125	150
	C2						
	C3						
	D1	XX-100-75-150		–	100	75	150
	D2						
	D3						
	E1	XX-100-100-100	No		100	100	100
	E2						
	E3						
	F1	XX-150-100-150			150	100	150
	F2						
	F3						
2	G1	XX-150-150-150			150	150	150
	G2						
	G3						
	H1	XR-150-150-150		2-10M	150	150	150
	H2						
	H3						

3.2 TEST SETUP AND PROCEDURE

The node tests were carried out on a self-reacting steel frame that was fastened to a post-tensioned slab. Following the traditionally used inverted loading scheme for corbel testing, the column reaction was applied as a load in the gravity direction while the beam reactions (carried by the corbels in the actual case) were represented by the reactions of the corbels on the supporting transverse steel beams, as illustrated in Fig. 4. A hydraulic actuator, with a load capacity and stroke of 500 kN and 355 mm, respectively, was used to apply the monotonic vertical load to the nodes. Furthermore, pinned supports were provided using 16-mm steel rods that were horizontally spaced from the corbel-column interface by the corbel's shear span, a. The actuator's built-in load cell and drawn-wire string potentiometers (SPs) were connected to a computerized data acquisition system (DAQ) were used to record the real-time load and corbel deflection values, respectively. Up until failure, the loading was delivered at a displacement-controlled rate of 0.25 mm/min.

https://doi.org/10.52202/080513-0421

Table 2: Mixing proportions of the UHPC

Component	Quantity (kg/m^3)	
	First phase	*Second phase*
Ce200SF-G^{TM} premix	2155.0	2294.3
Steel fibres[a]	156.0	155.4
cePAA1-80SDR[b]	12.9	13.2
Accelerator	_	11.9
Potable water	225.8	175.0

[a] *Fibre volume fraction is 2.0% by volume [18].*
[b] *Carbon nanofibers (CNF) paste [15].*

Table 3: Hardened properties of the UHPC

Material Property	*First phase*	*Second phase*
Compressive strength (MPa)[a]	130.6 $\pm$ 0.9	139.1 $\pm$ 2.4
Flexural strength (MPa)[a]	16.2 $\pm$ 0.7[b]	36.1 $\pm$ 2.2[c]

[a] *Performed as per the respective ASTM standards and ASTM C1856 [16].*
[b] *Obtained using 150 x 150 x 500 mm prisms as per ASTM C1609 [17].*
[c] *Obtained using 75 x 75 x 275 mm prisms as per ASTM C1856 [16].*

Figure 4: Test setup.

4 – NUMERICAL WORK

4.1 FINITE ELEMENT MODEL

The FEM models were developed in Abaqus [3] resembling the tested nodes and their boundary conditions. The eight-node linear brick solid element (C3D8R) was used to model the UHPC elements [19]. As seen in Fig. 5, the top 300 × 150 mm surface carried the weight, while the corbels were supported by a 20-mm wide surface centred with the mid-length of each corbel. To enable the model to function similarly to the experimental specimens, displacement boundary conditions were applied to the support plates. While the boundary conditions for the supports were defined using multi-point constraints (MPCs), the load was applied as a vertical downward displacement. A mesh size of 10 mm was used for the FEM models.

The properties of UHPC under compression and tension were defined using the concrete damage plasticity (CDP) model [20]. Table 4 lists the mechanical characteristics and CDP parameters of the UHPC implemented in the FEM [19]. The material models for UHPC in compression and tension were based on the studies from Ridha et al. [12] and Shafieifar et al. [21], respectively. To adequately model the load-deflection response of the prisms tested for flexural strength [12], the CDP model under tension was validated using reverse analysis [22]. Further details on the validation of the FEM can be found in a previous paper [23].

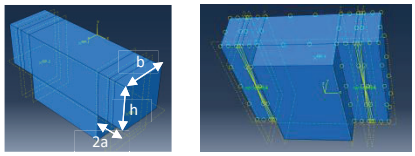

Figure 5: Details of FEM and boundary conditions.

4.2 PARAMETRIC STUDY

The parametric study included 79 FEM models, examined parameters: a) shear span, b) depth, c) width of the corbels, d) CDP model parameters-both tension and compression e) reinforcement ratio. The depth, width and shear span of the FEMs in the parametric study ranged between 100 to 250 mm, 150 to 500 mm, and 50 to 150 mm, respectively. It is worth noting that the variations in compressive and tensile strengths for UHPC are interrelated and can be adjusted by modifying the fibre dosage. However, this aspect (i.e., modelling different UHPC mixes with different fibre dosages) was not within the scope of this study. Instead, the variations of each CDP parameter were analysed separately i.e., keeping all other parameters constant as listed in Table 4 to assess its effect on the response of the UHPC nodes performance. It is advisable to validate the developed analytical models (discussed later) against FEMs created using actual concrete mixtures that exhibit different stress-strain behaviours in both compression and tension. For nodes reinforced with steel bars, closed vertical stirrups were modelled similar to tests. The dimensions of these nodes were chosen to meet the concrete cover and bar spacing requirements set forth in CSA A23.3-19 [24]. The properties of the steel bars utilized in the FEMs are detailed in Table 5.

Table 4: Material properties of materials used in FEM

UHPC		
Elastic Properties [19]		
Modulus of elasticity (MPa)	45,000	
Poisson's ratio	0.19	
CDP Model Parameters [19]		
Plasticity	Dilation angle	38°
	eccentricity	0.1
	fb0/fc0	1.1
	K	0.667
	Viscosity	0.0001
Compressive behaviour [12]	Yield strength (MPa)	Inelastic strain
	f_c = 125	0
	f'_c = 130	$\varepsilon_{pl,peak}$ = 0.003
	$f_{c,crush}$ = 40	$\varepsilon_{pl,crush}$ = 0.018
Tensile behaviour [21]	Yield strength (MPa)	Cracking strain
	$f_{t,cr}$ = 0.7	0

https://doi.org/10.52202/080513-0421

	$f_t = 9.3$	$\varepsilon_{pl,t} = 0.0035$
	$f_{t,r} = 2$	$\varepsilon_{pl,r} = 0.03$
Steel Bars		
Elastic Properties		
Modulus of elasticity (MPa)	200,000	
Poisson's ratio	0.3	
Plastic Response		
Tensile behaviour [12]	Yield strength (MPa)	Plastic strain
	400	0
	590	0.02

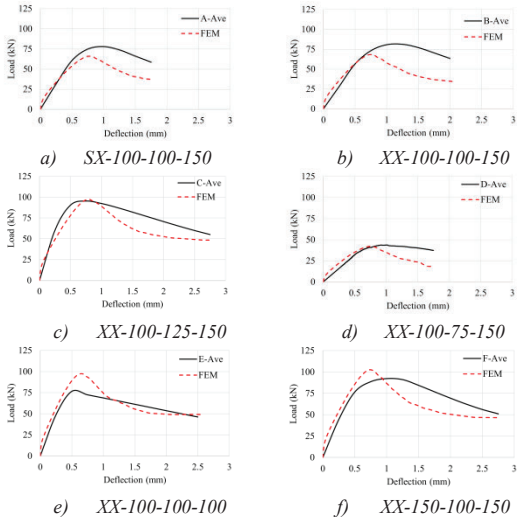

a) SX-100-100-150 b) XX-100-100-150

c) XX-100-125-150 d) XX-100-75-150

e) XX-100-100-100 f) XX-150-100-150

Figure 6: Average load-deflection response for the UHPFRC node replicates against FEM predictions.

5 – RESULTS

5.1 RESULTS FROM PHASE 1 TESTS

In general, the load-deflection response of the specimens exhibited a linear trend up to approximately 90% of the peak load capacity. Following this linear phase, the relationships started to show signs of softening as the load capacity of the corbels was approached. This softening behaviour is indicative of the material reaching its elastic limit, at which point the structures began to exhibit more pronounced deformation. Ultimately, this was followed by a descending branch in the load-deflection curve, which corresponds to the formation of a significant crack at the corner on the tension side of the corbel-column interface. An example of a node after testing are presented in Fig. 7a, where the dominant failure mode was in flexure at interface. This consistent failure mode suggests that the fibre reinforcement incorporated in the UHPC was no longer capable of bridging the cracks beyond this loading.

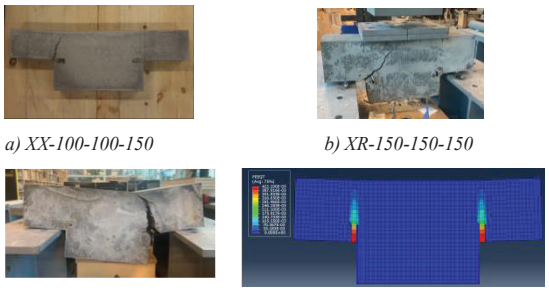

a) XX-100-100-150 b) XR-150-150-150

c) XX-150-150-150 d) XX-250-150-150

Figure 7: Examples of node failure in experiments and FEM.

A five-character alphanumeric designation is used to identify the tested nodes, with the first letter, S or X, indicated nodes with or without lower stub, respectively. Similarly, the second letter, R or X, denoted nodes with or without longitudinal corbel bars, respectively. In addition, the third, fourth and fifth numbers referred to the width, thickness, and length of the corbels, respectively. Notably, it was observed that increasing the corbel depth by 33% and 67% (as seen in specimens XX-100-100-150 and XX-100-125-150, respectively) significantly increased the load-carrying capacity by approximately 100% and 167% in comparison to XX-100-75-150. In contrast, increasing the corbel width by 50% in specimen XX-150-100-150 resulted in a peak load increase of only 16% compared to XX-100-100-150. This finding reinforces the notion that while both depth and width contribute to load capacity, an increase in depth is more effective.

On the contrary to initial calculations, a reduction in the shear span of the corbel did not result a significant impact on capacity. This observation suggests that the absence of steel bar reinforcement led to premature failure of the UHPC corbels. Additionally, it also indicates that higher shear effects were present, which caused the corbels to fail before they could reach their full flexural capacity. This finding suggests a need to limit the shear span-to-depth ratio of the UHPC corbels to a minimum of 0.75.

5.2 RESULTS FROM PHASE 2 TESTS

The load-deflection response of the nodes without bars in the second phase of testing followed the same behaviour as that for the nodes tested in the first phase. Due to the enhanced quality control in the second phase, consistent responses can be observed for the replicates as shown in Fig. 8. The average load capacity of the un-reinforced UHPC nodes was about 231 kN, exceeding the predicted value using the proposed analytical model (i.e., 172 kN – as discussed later). As shown in Fig. 7b, the un-reinforced UHPC nodes failed by flexure in a similar manner to the nodes in the first phase.

https://doi.org/10.52202/080513-0421

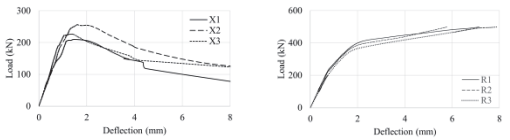

a) nodes without bars *b) bar-reinforced nodes*

Figure 8: Load deflection response of the UHPC nodes in the second phase of experiments.

The bar-reinforced nodes exhibited excellent performance, reaching the capacity of the actuator without failing. However, significant cracks formed vertically then propagated diagonally towards the loaded surface accompanied by some concrete crushing below the steel loading plate (Fig. 7c). Consistency between the different replicates was also noticed as evident in Fig. 8b. The average load capacity of the bar-reinforced nodes was assumed to be 405 kN, since the strain gauges (attached to the steel bars on the tension side near the corbel-column junction) showed yielding around that load value (Fig. 9). This agreed well with the predicted value using the developed model (i.e., 403 kN). This can be attributed to the fact that the load capacity of the bar-reinforced nodes is more dependent on the properties of the steel bars rather than UHPC which fails in the tension zone at much lower loads.

Overall, the results of the second phase confirmed the great potential of the developed nodes while reinforced with the simplest form of bar reinforcement, ensuring adequate structural integrity even at its ultimate state.

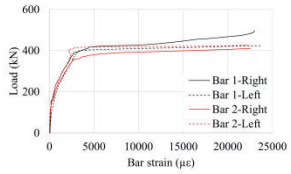

Figure 9: Load-strain response for the bar-reinforced UHPC node XR-150-150-150.

5.3 RESULTS OF PARAMETRIC STUDY

All FEMs, whether reinforced with steel bars or not, exhibited failure through a single vertical crack at the corbel-column interface, as illustrated in Fig. 7d. The load-deflections are plotted in Fig. 10, where both peak load and stiffness increased with the increase in corbel width, thickness, and with a reduction in shear span. Notably, the deflection at peak load remained fairly consistent across all modelled corbel widths, while it increased with greater thickness and shear span. Additionally, the post-peak response declined more steeply as the shear span of the corbel was reduced from 100 mm to 50 mm.

Altering the CDP parameters related to compression had a minor effect on the load-deflection behaviour of nodes without bars. In contrast, variations in the tensile parameters of the CDP model for UHPC significantly influenced the response of those nodes (Fig. 11), with cracking strength having the least impact and rupture strength showing the most notable effect. For example, enhancing the rupture strength to 4 MPa (approximately 50% of its peak tensile strength) for nodes without bars (Fig. 11b) resulted in a nearly flat post-peak load-deflection curve. This, along with other CDP parameter effects, highlights the necessity of understanding the entire stress-strain response in tension for UHPC nodes. Similar to the nodes without bars, modifying the CDP parameters in compression for bar-reinforced nodes resulted in negligible changes, primarily beyond the onset of flexural cracking. Comparably, adjustments to certain CDP parameters in tension, such as cracking strength and peak or ultimate strain, had minimal impact on the load-carrying capacity of bar-reinforced nodes. However, significant effects were observed by altering the peak (Fig. 11d) or rupture tensile strengths (Fig. 11e), highlighting the importance of accurately determining these properties for the UHPC in use (Fig. 12).

Figs. 10 and 11 reveals that introducing 2-10M steel bars led to a significant increase in load-carrying capacity, ranging from about 125% to 243%, depending on the geometry. As anticipated, the addition of steel bars provided ductility to the UHPC corbels, evident from the yielding plateau following the initial peak load. The effects of geometry on the bar-reinforced nodes followed similar trends as those without bars. As depicted in Fig. 12, an increase in the reinforcement ratio led to an increase in load capacity of up to 305%. It is also noteworthy that corbels reinforced with 10M bars demonstrated higher load-carrying capacity than those reinforced with 15M bars, keeping the same reinforcement ratio. This can be attributed to the larger surface area provided by a higher number of smaller 10M bars bonding to the UHPC.

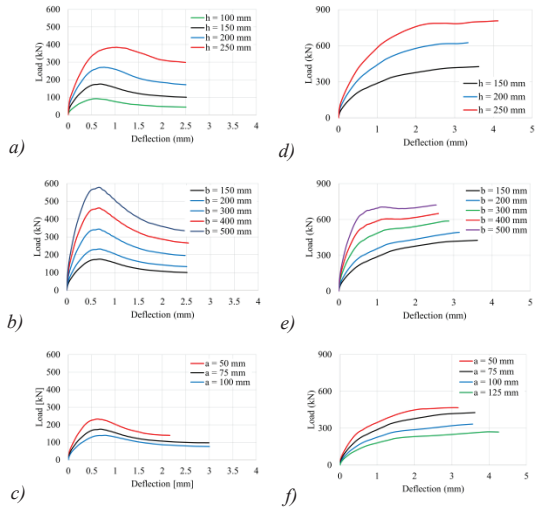

Figure 10: Effect of geometry on the response of UHPC node FEMs (a, b, and c: without bars, d, e, and f: with bars).

6 – ANALYTICAL MODELS

6.1 MODELS FOR NODES WITHOUT BARS

https://doi.org/10.52202/080513-0421

The load-carrying capacities of the FEMs without steel bars were estimated using Eq. (1). Additionally, the flexural model proposed by Fattuhi [11] was employed to estimate the load capacities of the FEMs.

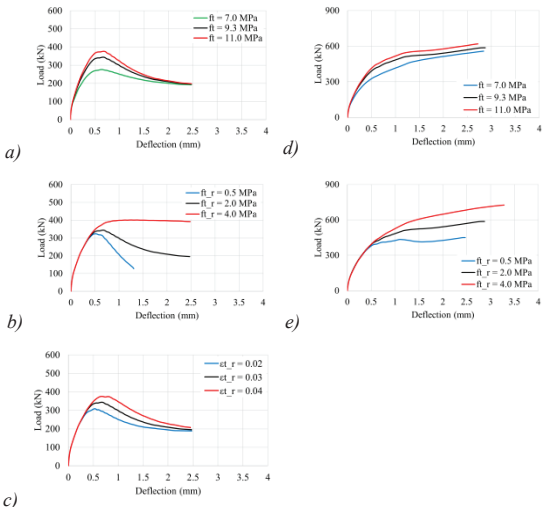

Figure 11: Effect of CDP tensile parameters on the response of UHPC node FEMs (a, b, and c: without bars, d and e: with bars).

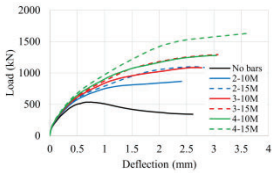

Figure 12: Effect of amount of reinforcement on the response of bar-reinforced UHPC node FEMs.

Based on the predicted load capacities using Eq. (1), the mean ratio of predicted to FEM load capacity was found to be 1.43 ± 0.15, with coefficients of variation (COV) and determination (R^2) of 10.6% and 0.95, respectively, as shown in Table 5, which indicates an overly estimated load capacity. A regression analysis was then conducted on the results of the FEMs, while suggesting that direct tensile strength be utilised instead of flexural strength. As a result, the load prediction equation is proposed to be revised as follows.

$$P_{flex,mod} = \frac{4.9 f_t^{0.7} b h^{1.6}}{3a^{0.7}} \quad (2)$$

where $P_{flex,mod}$ is the predicted load using the modified flexure equation, f_t is the direct tensile strength of the used UHPC. The mean predicted to FEM load capacity ratio using Eq. (2) was 1.01 $\pm$ 0.02, with coefficients of variation (COV) and determination (R^2) of 2.2% and 0.997, respectively.

The flexural model proposed by Fattuhi [11] underestimated the load capacity of the FEMs, yielding a mean predicted-to-FEM ratio of 0.67 ± 0.11, as shown in Table 5. Due to the complexity of this model where it was difficult to isolate each parameter to study its effect, it was determined that the k_o factor, which represents the assumption of uniform tensile stresses across the tension zone of the cross-section, should be established as the primary controlling factor. The regression analysis of the k_o factor in relation to each parameter led to the development of the following empirical formula.

$$k_{o,\,mod} = 1.86\text{E-}10\ (43990 - b)\ (534 - h)\ (a + 198)\ (f_t^{-0.3}) \quad (3)$$

where f_t is in MPa and all other parameters are in mm. Using this modified factor from Eq. (3), the mean predicted-to-FEM load ratio was 1.03 $\pm$ 0.04, with coefficients of variation (COV) and determination (R^2) of 3.5% and 0.99, respectively.

6.2 MODELS FOR BAR-REINFORCED NODES

The load predictions based on the model by El-Helou and Graybeal [13] were higher than those estimated by the FEMs, yielding a mean predicted-to-FEM ratio of 1.22 ± 0.17, with coefficients of variation (COV) and determination (R^2) of 14.2% and 0.93, respectively. Consequently, it was decided to adjust the reduction factor γ to account for possible variations in tensile behaviour associated with the different considered. A regression analysis was conducted on the studied parameters, leading to the proposal of the following formula.

$$\gamma_{mod} = 2.6\text{E-}07\ (967 - b)\ (387 - h)\ (a - 8)\ (f_t^{-0.7}) \leq 1.0 \quad (4)$$

Equation (4) was applied in El-Helou and Graybeal's model to recalculate the load capacities of the FEMs. As shown in Table 6, the resulted mean predicted-to-FEM load ratio was 0.97 ± 0.04, with coefficients of variation (COV) and determination (R^2) of 4.0% and 0.99, respectively.

In contrast, the flexural model proposed by Fattuhi [11] underestimated the load capacity of the FEMs, yielding a mean predicted-to-FEM ratio of 0.9 ± 0.1, which aligns with the predictions made for the nodes without bars. Consequently, it was decided to adjust the k_o factor based on the variations in the parameters, leading to the development of the following empirical formula.

$$k_{o,\,mod} = 1.3\text{E-}09\ (1155 - b)\ (433 - h)\ (-a^2 + 241a - 6031)\ (f_t^{-0.7}) \quad (5)$$

Using this modified factor in Fattuhi's model to predict the load capacities of the FEMs, as shown in Table 6, the mean predicted-to-FEM load ratio of 0.99 ± 0.04, with coefficients of variation (COV) and determination (R^2) of 3.6% and 0.99, respectively.

The revised models of Fattuhi [11] and El-Helou and Graybeal [13] were used to estimate the load capacities of the FEMs reinforced with varying amounts of steel bars.

As illustrated in Table 7, these models predicted the load capacities of the FEMs with reasonable accuracy.

8 – CONCLUSION

This study introduces a novel concept of precast ultra high-performance concrete (UHPC) nodes for post-and-beam timber gravity load frames, providing superior performance, adequate fire resistance, ease of installation, and cost reduction.

- The experimental results from the tested nodes demonstrated satisfactory performance in terms of…, which can be further improved when steel bars were added as longitudinal reinforcement.
- A parametric study was performed using a developed FEM, where non- linear relationships were observed between geometry and node load-carrying capacity.
- Altering the CDP parameters in compression had minimal impact on the load-deflection response of the nodes.
- Changes to the CDP parameters in tension significantly affected the load-deflection response of the nodes.
- The inclusion of steel bars resulted in a substantial increase in load capacity of up to 243%. Increasing the number of bars significantly raised the load capacity of the nodes.
- Altering the CDP parameters in compression had minimal impact on the load-deflection response of the nodes.
- Altering the CDP parameters in compression had minimal impact on the load-deflection response of the nodes.
- Changes to the CDP parameters in tension significantly affected the load-deflection response of the nodes.
- The inclusion of steel barsresulted in a substantial increase in load capacity of up to 243%. Increasing the number of bars significantly raised the load capacity of the nodes.
- The models proposed by Fattuhi et al. [11] and El-Helou and Graybeal [13] were found to provide poor estimates of load capacity for the FEMs in the parametric study. Through reverse calculations and regression analysis, new proposed formulas were with enhanced accuracy.
- The promising potential of the developed UHPC nodes was confirmed through a second phase of experimental tests where steel-bar reinforced nodes were tested. The tests demonstrated the structural integrity of the nodes under the highest applied load.

9 – ACKNOWLEDGEMENT

The authors wish to express their heartfelt gratitude to the Mitacs Accelerate Fellowship and Fast + Epp for financially supporting this study. They also greatly appreciate the technical assistance provided by the staff at Fast + Epp's Concept Lab at and the University of British Columbia Okanagan. Special thanks are extended to Sanderson Concrete Corp. for facilitating fabricating the specimens. The expertise offered by Mr. Vic Perry of ceEntek Pte Ltd. Throughout the experimental program is highly valued. Additionally, the assistance provided by Dr. Zahra Mohammadi with material testing is sincerely appreciated.

Table 5: Numerical and analytical results of the nodes without bars (loads in kN)

Specimen ID	P_{FEM}	P_{flex}	P_{flex}/P_{FEM}	$P_{Fattuhi}$	$P_{Fattuhi}/P_{FEM}$	$P_{flex,mod}$	$P_{flex,mod}/P_{FEM}$	$P_{Fattuhi,mod}$	$P_{Fattuhi,mod}/P_{FEM}$
X150-150-100	232.3	364.5	1.57	208.4	0.90	228.9	0.99	241.5	1.04
X150-150-150	175.3	243	1.39	138.9	0.79	172.3	0.98	176.7	1.01
X150-150-200	139.7	182.3	1.30	104.2	0.74	140.9	1.01	144.1	1.03
X150-100-150	91.8	108	1.18	61.75	0.67	90.1	0.98	88.3	0.96
X150-200-150	271.0	432	1.59	247.0	0.91	273.0	1.01	274.5	1.01
X150-250-150	384.2	675	1.76	385.9	1.00	390.1	1.02	366.4	0.95
X200-150-150	232.7	324	1.39	185.3	0.80	229.7	0.99	235.23	1.01
X250-150-150	290.4	405	1.39	231.6	0.80	287.2	0.99	293.8	1.01
X300-150-150-7	275.8	365.8	1.33	217.5	0.79	282.5	1.02	296.0	1.07
X300-150-150-9.3	323.4	486	1.50	277.9	0.86	344.6	1.07	352.1	1.09
X300-150-150-11	376.3	574.8	1.53	337.5	0.90	387.6	1.03	394.8	1.05
X350-150-150	404.1	567	1.40	324.2	0.80	402.1	0.99	410.4	1.02
X400-150-150	462.1	648	1.40	370.5	0.80	459.5	0.99	468. 5	1.01
X500-150-150	578.2	810	1.40	463.1	0.80	574.4	0.99	584.3	1.01
Mean			1.43		0.82		1.00		1.03
SD			0.15		0.08		0.02		0.04
COV%			10.6		10.3		2.2		3.5
R^2			0.95		0.95		0.997		0.99

https://doi.org/10.52202/080513-0421

where P_{FEM} = load capacity of the FEM model of the node, P_{flex} = load capacity of the node as per Eq. 1, $P_{Fattuhi}$ = load capacity of the node as per Fattuhi's [11] model, $P_{flex,mod}$ = load capacity of the node as per Eq. 2, and $P_{Fattuhi,mod}$ = load capacity of the node as per Fattuhi's [11] model using modified k_o factor as per Eq. 3.

Table 6: Numerical and analytical results of nodes reinforced with two 10M bars (loads in kN)

Specimen ID	P_{FEM}	$P_{El\text{-}Helou}$	$P_{El\text{-}Helou}/P_{FEM}$	$P_{Fattuhi}$	$P_{Fattuhi}/P_{FEM}$	$P_{El\text{-}Helou,mod}$	$P_{El\text{-}Helou,mod}/P_{FEM}$	$P_{Fattuhi,mod}$	$P_{Fattuhi,mod}/P_{FEM}$
R150-150-100	466.5	677.0	1.45	545.6	1.17	499.2	1.07	501.0	1.07
R150-150-120	466.3	564.2	1.21	454.7	0.98	450.5	0.97	464.56	0.97
R150-150-150	426.5	451.3	1.06	363.8	0.85	400.9	0.94	416.5	0.98
R150-150-180	367.4	376.1	1.02	303.1	0.83	367.3	0.99	373.4	1.02
R150-150-200	333.6	338.5	1.01	272.8	0.82	338.5	1.01	346.5	1.04
R150-150-250	270.6	270.8	1.01	218.3	0.81	270.8	1.01	283.8	1.05
R150-150-300	225.4	225.7	1.01	181.9	0.81	225.7	1.01	224.9	0.99
R150-200-150	625.7	771.2	1.23	578.9	0.93	604.3	0.97	616.6	0.99
R150-250-150	807.4	1140.2	1.41	825.9	1.02	759.8	0.94	793.0	0.98
R200-150-150	491.7	546.0	1.11	412.8	0.84	461.9	0.94	472.2	0.96
R250-150-150	536.2	639.7	1.19	461.4	0.86	514.0	0.96	521.1	0.97
R300-150-150-7	557.9	614.6	1.10	442.6	0.79	526.7	0.94	536.1	0.96
R300-150-150-9.3	587.4	732.6	1.25	509.7	0.87	556.9	0.95	563.1	0.96
R300-150-150-11	608.7	818.6	1.34	558.7	0.92	575.9	0.95	580.2	0.95
R350-150-150	613.3	825.6	1.29	557.9	0.91	591.1	0.96	598.57	0.98
R400-150-150	650.1	918.3	1.41	606.0	0.93	616.4	0.95	627.36	0.97
R500-150-150	721.0	1103.9	1.53	702.0	0.97	640.0	0.89	664.97	0.92
Mean			1.22		0.90		0.97		0.99
SD			0.17		0.10		0.04		0.04
COV%			14.2		11.0		4.0		3.6
R^2			0.93		0.92		0.99		0.99

where $P_{El\text{-}Helou}$ = load capacity of the node as per the procedure by El-Helou and Graybeal [13], $P_{Fattuhi}$ = load capacity of the node as per Fattuhi's [11] model, $P_{El\text{-}Helou,mod}$ = load capacity of the node as per the procedure by El-Helou and Graybeal [13] using modified γ factor as per Eq. 4, and $P_{Fattuhi,mod}$ = load capacity of the node as per Fattuhi's [11] model using modified k_o factor as per Eq. 5.

Table 7: Numerical and analytical results of nodes with different amounts of bar reinforcement (loads in kN)

Specimen ID	P_{FEM}	$P_{El\text{-}Helou,mod}$	$P_{El\text{-}Helou,mod}/P_{FEM}$	$P_{Fattuhi,mod}$	$P_{Fattuhi,mod}/P_{FEM}$
R300-200-150-2-10M	866.1	818.2	0.95	830.4	0.96
R300-200-150-3-10M	1085.1	963.4	0.89	991.8	0.91
R300-200-150-4-10M	1278.3	1107.5	0.87	1151.9	0.90
R300-200-150-2-15M	1076.5	1107.6	1.03	1151.9	1.07
R300-200-150-3-15M	1293.2	1392.6	1.08	1468.4	1.14
R300-200-150-4-15M	1635.4	1673.8	1.02	1779.8	1.09
Mean			0.97		1.01
SD			0.08		0.09
COV%			7.95		8.95
R^2			0.897		0.897

where $P_{El\text{-}Helou,mod}$ = load capacity of the node as per the procedure by El-Helou and Graybeal [13] using modified γ factor as per Eq. 4, and $P_{Fattuhi,mod}$ = load capacity of the node as per Fattuhi's [11] model using modified k_o factor as per Eq. 5.

10 – REFERENCES

[1] M. Mulder, C. Dickof, R. Jackson, and J. Kim. "Case Study: A HIGH-RISE TIMBER BRACED AND CLT SHEARWALL BUILDING IN VANCOUVER, BRITISH COLUMBIA." In: Canadian Conference - Pacific Conference on Earthquake Engineering, Vancouver, British Columbia, 2023.

[2] T. Hozjan, C. Bedon, A. Ogrin, M. Cvetkovska, and M. Klippel. "Literature review on timber–concrete composite structures in fire." In: Journal of Structural Engineering, 145.11 (2019), 04019142 p.

[3] Dassault Systèmes Simulia Corporation. (2017). "ABAQUS Analysis User's Manual, Version 6.14-5.".

[4] S. Hehl, T. Tannert, R. Meena, and T. Vallee. "Experimental and Numerical Investigations of Groove Connections for a Novel Timber-Concrete-Composite System." In: Journal of Performance of Constructed Facilities 28.6 (2014), A4014010 p.

[5] Md. Shahnewaz, R. Jackson, and T. Tannert. "CLT Concrete Composite Floors with Steel Kerf Plate Connectors." In: Construction and Building Materials 319 (2022), 126092 p.

[6] J. Hartig, P. Haller, and A. Heiduschke. "Holzfachwerke mit Verbindungsknoten aus Beton: Teil 1: Konzept und experimentelle Untersuchungen." In: Bautechnik 90.1 (2013), pp. 1-8.

[7] J. H. Negrão, L. D. Brito, A. G. Dias, C. C. Júnior, and F. R. Lahr. "Numerical and experimental study of small-scale moment-resistant reinforced concrete joints for timber frames." In: Construction and Building Materials 118 (2016), pp. 89-103.

[8] Canadian Standards Association. CSA S16-19. "Design of steel structures.", Toronto, ON, 2019.

[9] R. Solhmirzaei, V. K. R. Kodur, S. and Banerji. "Shear behavior of ultra high performance concrete beams without stirrups." In: International Interactive Symposium on Ultra-High Performance Concrete 2.1, Iowa State University Digital Press, 2019.

[10] S. Choi, C. Joh, and S. C. Chun. "Behavior and strengths of single cast-in anchors in Ultra-High-Performance Fiber-Reinforced Concrete (UHPFRC) subjected to a monotonic tension or shear." In: KSCE Journal of Civil Engineering 19.4 (2015), pp. 964–973.

[11] N. I. Fattuhi. "Strength of FRC corbels in flexure." In: J. Struct. Eng. 120.2 (1994), pp. 360-377.

[12] M. M. Ridha, N. T. Al-Shafi'i, and M. M. Hasan. "Ultra-high performance steel fibers concrete corbels: Experimental investigation." In: Case studies in construction materials 7 (2017), pp. 180-190.

[13] R. G. El-Helou, and B. A. Graybeal. "Flexural behavior and design of ultrahigh-performance concrete beams." In: J. Struct. Eng. 148.4 (2022), 04022013 p.

[14] A. Abdallah, Md. Shahnewaz, C. Dickof, and L. Tobber. "Production of UHPFRC nodes for timber structures in the Canadian West Coast: Lessons learned." In: CSCE Annual Conference, Niagara Falls, ON, Canda, June 5-7, 2024.

[15] ceEntek Pte Ltd. "ce200SF-G™ —Technical data sheet." ceEntek Canada Ltd. Calgary, AB, Canada, 2021.

[16] American Society for Testing Materials International. ASTM C1856-17. "Standard practice for fabricating and testing specimens of ultra-high performance concrete." West Conshohocken, PA, 2017.

[17] American Society for Testing Materials. ASTM C1609-19. "Standard Test Method for Flexural Performance of Fiber-Reinforced Concrete (Using Beam with Third-Point Loading)." West Conshohocken, PA, 2019.

[18] American Concrete Institute. ACI PRC 544-18. "Guide to Design with Fiber-Reinforced Concrete." Farmington Hills, MI, 2018.

[19] S. Bahij, S. K. Adekunle, M. Al-Osta, S. Ahmad, S. U. Al-Dulaijan, and M. K. Rahman. "Numerical investigation of the shear behavior of reinforced ultra-high-performance concrete beams." In: Structural Concrete 19.1 (2018), pp. 305-317.M.

[20] J. Lubliner, J. Oliver, S. Oller, and E. Onate. "A plastic-damage model for concrete." In: Int. J. Solids Struct. 25.3 (1989), pp. 299–326.

[21] Shafieifar, M. Farzad, and A. Azizinamini, "Experimental and numerical study on mechanical properties of Ultra High Performance Concrete (UHPC)." In: Construction and Building Materials 156 (2017), pp. 402-411.

[22] S. T. Kang, Y. Lee, Y. D. Park, and J. K. Kim, "Tensile fracture properties of an Ultra High Performance Fiber Reinforced Concrete (UHPFRC) with steel fiber." In: Composite structures 92.1 (2010), pp. 61-71.

[23] A. Abdallah, Md. Shahnewaz, C. Dickof, and L. Tobber. "The behaviour of precast UHPC nodes for timber structures: A numerical study." In: 4th International Conference on New Horizons in Green Civil Engineering (NHICE-04), Victoria, BC, Canada, August 26 – 28, 2024.

[24] Canadian Standards Association. CSA A23.3:19. "Design of concrete structures.", Toronto, ON, 2019.

https://doi.org/10.52202/080513-0421